Research Square

Preprints are preliminary reports that have not undergone peer review.
They should not be considered conclusive, used to inform clinical practice,
or referenced by the media as validated information.

Histological, Immunohistochemical, and Radiographic Evaluation of Chick Femur Osteogenesis Following in Ovo Calcium Carbonate Nanoparticles Administration

Lamyaa Hadi

lamyaahadi2016@nahrainuniv.edu.iq

Al-Nahrain University

Hayder Jawad Kadhim

Al-Nahrain University

Fatma Ayadi

University of Sfax

Article

Keywords: Chick embryo, calcium carbonate nanoparticles, femur, osteogenesis, osteocalcin, sialoprotein, immunohistochemistry, radiography

Posted Date: July 7th, 2026

DOI: https://doi.org/10.21203/rs.3.rs-9868562/v1

License: This work is licensed under a Creative Commons Attribution 4.0 International License.
Read Full License

Additional Declarations: No competing interests reported.

Histological, Immunohistochemical, and Radiographic Evaluation of Chick Femur Osteogenesis Following in Ovo Calcium Carbonate Nanoparticles Administration

Lamyaa Hadi[1,] *, Hayder Jawad Kadhim[1], Fatma Ayadi[2]

[1] Department of Human Anatomy, College of Medicine, Al-Nahrain University, Baghdad, Iraq; lamyaahadi2016@nahrainuniv.edu.iq (L.H); haider_kadhim@yahoo.com (H.J.K)
[2] Research Laboratory LR[19]ES[13], Faculty of Medicine of Sfax, University of Sfax, Sfax, Tunisia; ayadi_fatma@medecinesfax.org (F.A)
* Correspondence: lamyaahadi2016@nahrainuniv.edu.iq

Abstract

This study presents histological, immunohistochemical, and radiographic evaluation of the effects of calcium carbonate nanoparticles (CCN) on femoral osteogenesis in chick embryos. A total of 100 fertilized eggs were used for histological and immunohistochemical analysis, and 120 eggs for radiographic assessment. Eggs were divided into control and experimental groups. Controls received pre-incubation injection of normal saline, while experimental groups were administered 0.2 mL of CCN suspension (500 μg/mL per egg).

Histological findings showed an advanced developmental configuration in the femoral diaphysis induced by CCN. Embryonic days 13 and 14 were most suitable for demonstrating morphological changes in the developing femur. Immunohistochemical analysis revealed a significant increase in osteocalcin and sialoprotein expression in femoral trabeculae of the experimental group compared with controls, indicating accelerated developmental progression in the femoral diaphysis.

Radiographic analysis showed a significant increase in mean grey values at day 13 in the experimental group, followed by a decrease at day 14 compared with controls. From days 15 to 18, mean grey values gradually increased in the experimental group, reflecting progressive bone mineralization.

Overall, these findings indicate that CCN enhance bone histogenesis and promote mineral deposition in the developing chick femur.

Keywords: Chick embryo; calcium carbonate nanoparticles; femur; osteogenesis; osteocalcin; sialoprotein; immunohistochemistry; radiography.

1. Introduction

The human femur develops through endochondral ossification, where bone forms from a cartilage template with progressive histological remodeling. Early femoral cartilage shows defined regions before diaphyseal ossification begins [1,2]. The femoral epiphysis contains organized cartilage zones, and secondary ossification centers later develop in the distal epiphysis. Long bone development occurs in two main phases: formation of a cartilage model and its replacement by bone through calcified cartilage. In the diaphysis, osteoblast differentiation, osteoid deposition, mineralization, and vascular invasion occur, followed by gradual replacement of calcified cartilage by bone. Osteoblasts arise from osteoprogenitor cells in the

perichondrium and periosteum, with osteogenic differentiation following chondrogenesis during skeletal development [5–9].

Bone formation biomarkers in tissue and circulation reflect osteogenic activity. Markers such as bone sialoprotein (BSP), osteocalcin, and osteonectin are associated with osteoblast differentiation and function. These non-collagenous proteins contribute to extracellular matrix mineralization and support adhesion and maturation of bone-forming cells, serving as indicators of osteogenesis [10].

Radiographic assessment is important in diagnosing bone disorders and evaluating skeletal health [11,12]. Although MRI and CT provide advanced imaging, conventional radiography remains essential for detecting structural changes that may not be evident with other modalities. Combining radiography with CT or MRI improves early detection and management of metabolic bone diseases [12,13]. These disorders reduce bone density and mineralization, leading to skeletal deformities and increased fracture risk [14]. Osteoporosis, the most common metabolic bone disease, is classified into primary and secondary forms. Primary osteoporosis includes postmenopausal (Type I) and senile (Type II) types. Type I is mainly linked to estrogen deficiency and accelerated trabecular bone loss, while Type II affects both trabecular and cortical bone and is associated with fractures of the hip, proximal humerus, tibia, and pelvis [15,16]. Radiographic features include cortical thinning, endosteal resorption, and reduced trabecular pattern [15].

Bone strength depends largely on bone mineral density (BMD), commonly measured by dual-energy X-ray absorptiometry (DXA). However, fracture resistance also depends on mineral distribution within the bone matrix. Excess mineralization may reduce bone toughness and increase fracture risk in highly mineralized regions [16,17]. Advanced 3D imaging improves bone biomechanics assessment, while methods such as ashing, microradiography, and electron microscopy remain destructive and limited in 3D analysis [18].

This study aimed to evaluate the effects of in ovo inoculation (IOI) of calcium carbonate nanoparticles (CCN) on chick embryo bone development using histological, immunohistochemical, and radiographic methods. Osteocalcin and sialoprotein immunostaining, together with radiographic bone density analysis, were used to assess osteogenesis and mineralization. The hypothesis was that nanoscale calcium carbonate enhances bone formation due to improved biological availability.

2. Materials and Methods

2.1. Nano calcium carbonate preparation

Calcium carbonate ($CaCO_3$) nanoparticles were synthesized by mixing 0.1 M Na_2CO_3 and 0.1 M $CaCl_2$ for 10 min, then centrifuged at 10,000 rpm and drying at 80°C. Nano-$CaCO_3$ powder sourced from f XFNANO Materials Tech Co., Ltd. (Jiangsu, China). According to the manufacturer, average size from 50–100 nm with >95% purity, bulk density 0.45 g/mL, and pH 9.5–10.

2.2. Histological and immunohistochemical analyses

For histological and immunohistochemical analyses, 100 fertilized chick eggs were used, whereas 120 fertilized eggs were used for the radiographic assessment. In both experiments, eggs were divided into control and experimental groups. The control groups received a pre-incubation injection of normal saline, while the experimental groups were administered a 0.2 mL suspension of CCN at 500 μg/mL per egg.

Two holes were made at the wider pole of each egg using a pointed instrument. The normal saline and hydrocolloid of CCN (for the control and experimental groups, respectively) were inoculated during the first day of incubation under sterile conditions into the albumen via the air sac of each egg through one of these holes using 27gauge, 20-mm needles. The hole was sealed using sterile tape, and the eggs were placed in an incubator immediately after the injection at standard incubation conditions, including the temperature 37.8C^0, humidity 55%, and turned frequently, fertilized chick eggs were obtained from the Poultry Research Station, Ministry of Agriculture, Baghdad, Iraq.

The incubation period was determined till the beginning of ossification in the femur's cartilage for 13 and 14 days. The removal of the eggshell is followed by excision of the membranes and extraction of the embryo [19]. The hind limbs collected were prepared for serial sagittal paraffin sectioning at a thickness of 5 μm according to a method reported by [20]. The routine hematoxylin and eosin staining was used for the sections prepared for the histological study.

The sections used for immunohistochemical labeling were processed using the IHC Detection Kit. The immunolabeled sections were photographed, and the images were analyzed using the Aperio ImageScope software (version 11.1.2.760). Primary antibodies included anti-osteocalcin and anti-sialoprotein.

Radiographic evaluation of the hind limbs of the extracted embryos was performed for both groups (control, experimental) at the following incubation periods (days 13^{th}, 14^{th}, 15^{th}, 16^{th}, 17^{th} and 18^{th}). The total number of embryos involved is 120, with 10 embryos for each period. One of the hind limbs from each embryonic period was removed and immediately fixed in 10% Neutral-Buffered Formalin (NBF) and saved in small containers [20].

2.3. The X-ray method

The X-ray machine specifications were those (Radiography Frame, Mindray Animal Core Model: VetixP8). The exposure factors were at energy (200-240 V), 50/50 Hz, 16 A (MAX.), 3.5 kW. The methodology of radiographic evaluation of the developing femurs was designed according to the concept established decades ago that digital processing of radiographic images is a common practice in clinical and experimental research [21]. Therefore, the development and mineralization of the femur bones were quantified in this study by processing digital radiographs of chick embryo hind limbs to estimate grey values in these bones. The grey values are the feature used for evaluation in most graphic analysis software, including the free-of-charge ImageJ 1.55d software (Wayne Rasband and contributions National Institutes of Health, USA. http://imagej, USA.org Java 1.8.0-345 (64-bit) 7233k of 12225MB) used in this study. The grey values in this software are saved in an 8-bit color space, and every pixel obtains a value between zero and 255. The zero value stands for black radiologic density, while 255 represents white total x-ray absorption. The analysis of the mean grey values needs the uncompressed file format, like TIFF, as compressed formats like JPG summarize areas of similar grey values, leading to loss of contrast and significant changes in mean grey values. The grey values are related to the absorption of X-rays [22].

This radiographic study involved evaluating mean grey values in the paracentral regions of the femur. The parameters obtained from these parts of the bones of the control group were compared with those obtained from the bones of the experimental group.

The assessment of radiographic images of the femur in terms of relative bone density, depending on the mean grey values, allowed the elucidation of more advanced developmental stages (including stages of 13, 14, 15, 16, 17, 18 day after incubation). The comparison of the

relative bone density of the control and experimental groups was the objective of reaching a conclusive impression of the effect of CCN on the maturation and mineralization of the femur.

2.4. Ethical approval:

All experimental procedures involving chick embryos were approved by the Research Ethical Committee of the College of Medicine, Al-Nahrain University (Approval Nos: 20250375, 20250376, 20250373). All experiments were conducted in accordance with the institutional and national guidelines for the care and use of laboratory animals. For this type of study, formal consent was not required.

3. Results

3.1. Histological description of the developing femur

3.1.1. Histology of femur of the control group at day 13 of incubation

Sagittal sections showed cartilaginous tissue at the proximal and distal diaphyseal regions. In contrast, the paracentral region contained longitudinal developing trabeculae and a marrow cavity, which appeared narrower toward the periphery.

The central diaphysis exhibited curved multilayered trabeculae with bilateral convexities that constricted the marrow cavity. Their peripheral margins formed longitudinal bony bands (Figures 1A, B). At higher magnification, hypertrophic chondrocytes formed the core between curved trabeculae, while lightly stained hypertrophic chondrocytes delineated the marrow boundary (Figure 1C). Marrow cells were intermingled with hypertrophic chondrocytes at the cartilage interface, where chondrocyte nuclei were often seen near the boundary between marrow and cartilage (Figure 1D).

The circumferential region between trabeculae contained osteoprogenitor cells with spindle-shaped morphology and flattened nuclei. Polygonal osteoblasts were also present at peripheral regions, occupying spaces between trabeculae, particularly near longitudinal bony bands at the diaphyseal margins (Figure 1E). Marrow spaces contained blood vessels and densely packed hematopoietic precursor cells. The marrow cavity was surrounded by osteoblasts, cartilage tissue, and multinucleated osteoclasts, with some vessels containing erythropoietic cell aggregates (Figure 1F).

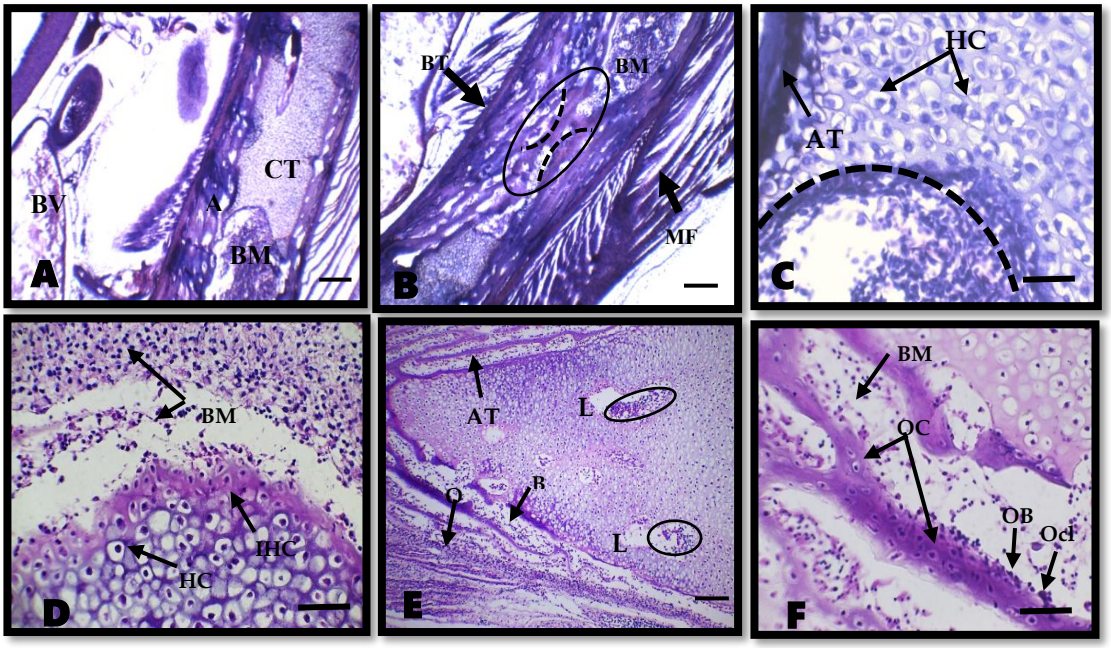


Figure 1. Sagittal sections of femur in control chick embryos at day 13 of incubation. (A) Distal diaphysis showing cartilaginous tissue (CT), bone marrow space (BM), blood vessels (BV), and arching trabeculae (AT). (B) Paracentral femoral shaft showing muscle fibers (MF), blood vessels (BV), outer longitudinal bony trabeculae (BT), central marrow cavity region (black circle), and narrowed marrow cavity with multilayered arching trabeculae (dotted lines). (C) Hypertrophic chondrocytes (HC) forming the core between arching trabeculae and outlining the marrow cavity boundary. (D) Hypertrophic chondrocytes (IHC) mixed with marrow cells at the cartilage–marrow interface. (E) Osteoprogenitor cells (OP) within trabeculae and osteoblasts along peripheral bony trabeculae. (F) Bone marrow spaces containing hematopoietic cells, blood vessels, osteoblasts (OB), osteoclasts (Ocl), and osteocytes (OC). H&E staining. Magnification: (A, B ×40), (E ×100), (C, D, F ×400). Data represent mean ± SD (n = 10 per group).

3.1.2. Histology of femur of the control group at day 14 of incubation

Sagittal sections showed extensive trabecular formation throughout the diaphysis, with variable-sized intertrabecular spaces (Figure 2A). Hypertrophic cartilage was observed at the proximal and distal regions of the diaphysis (Figure 2B).

Trabecular formation produced a spongy-like pattern, while hematopoietic and vascular elements occupied the intertrabecular spaces of the proximal and distal diaphysis (Figure 2C). The central diaphyseal region showed peripheral compact trabeculae bordered by periosteal tissue containing cellular and acellular components. Osteoprogenitor cells were present within the periosteal tissue surrounding the diaphysis (Figure 2D).

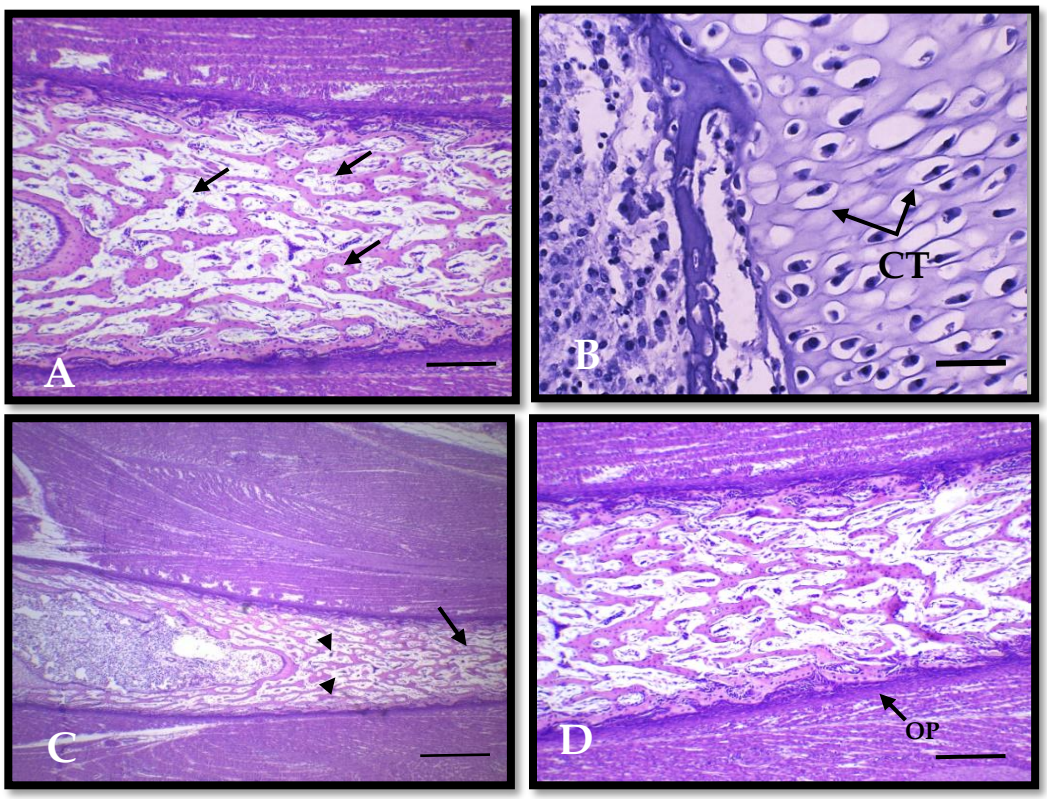


Figure 2. Sagittal sections of femur in control chick embryos at day 14 of incubation. (A) Diaphyseal shaft showing variable intertrabecular spaces filled with hematopoietic tissue.

(B) Distal diaphysis showing hypertrophic cartilage (CT) and hematopoietic cells within intertrabecular spaces. (C) Distal diaphyseal trabeculae forming a spongy pattern (arrow), with wider central cavitation (arrowhead). (D) Osteoprogenitor cells (OP) within periosteal tissue. H&E staining. Magnification: (A, D ×100), (C ×40), (B ×400). Data represent mean ± SD (n = 10 per group).

3.1.3. Histology of femur of the experimental group at day 13 of incubation

Marked changes in the arching multilayered pattern were observed in the paracentral region of the femoral shaft compared with the control group. This region was largely occupied by trabecular bone and marrow tissue (Figure 3A), resembling the control group at day 14, indicating advanced diaphyseal development. Enlarged marrow spaces containing hematopoietic cells were also present. The periosteal layer surrounded the diaphysis (Figure 3B). At higher magnification, mineralized bone matrix containing osteocytes within lacunae, along with osteoblasts and osteoclasts involved in bone remodeling, was observed (Figures 3C, D). These features were absent in the control group at the same stage.

In contrast to the control group, which showed cartilage at the proximal and distal diaphyseal regions, the experimental group exhibited cup-shaped trabeculae near the epiphyseal plate (Figure 3E). Higher magnification showed bone matrix containing osteocytes, osteoblasts, and osteoclasts. Sections also revealed an ossification zone adjacent to a cartilage zone, with hypertrophic chondrocytes near calcified cartilage (Figure 3F).

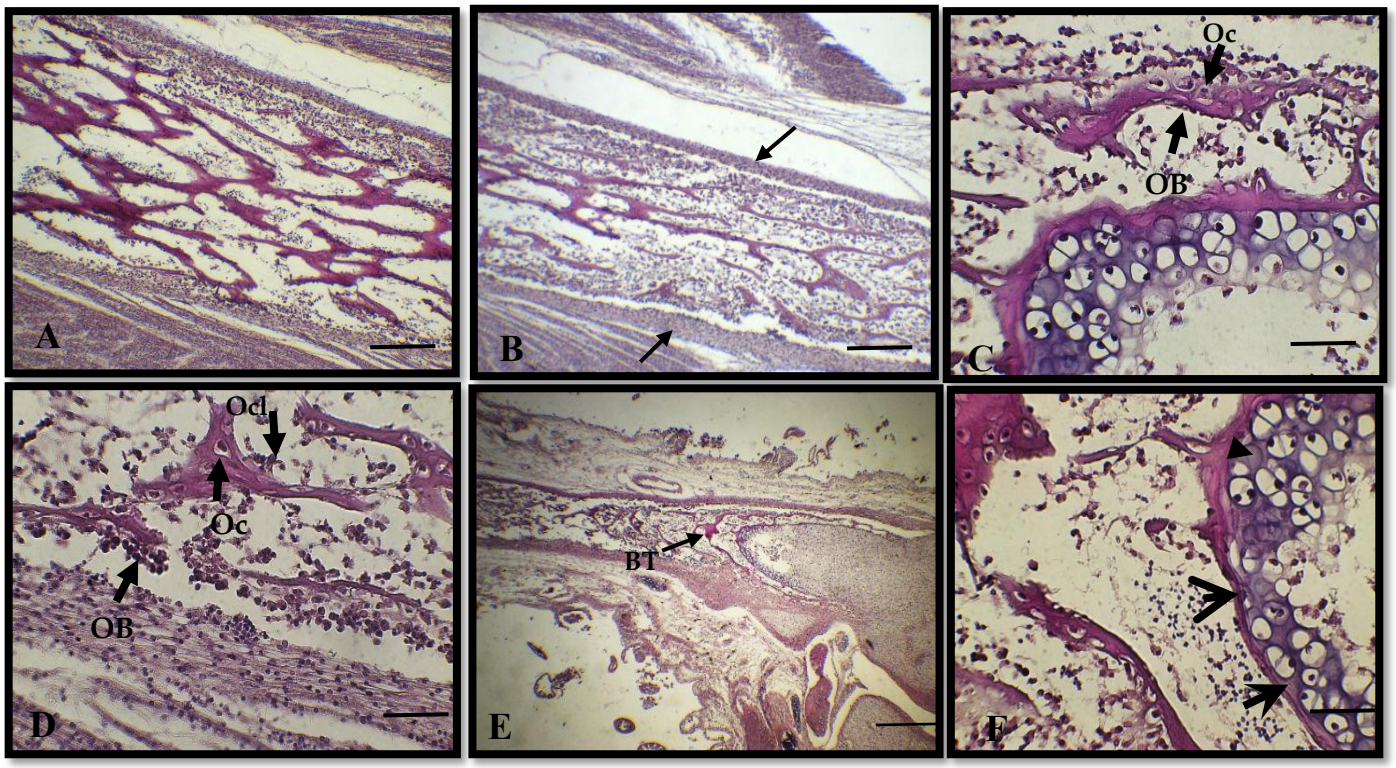


Figure 3. Sagittal sections of femur in experimental chick embryos at day 13 of incubation. (A) Paracentral femoral shaft containing trabecular bone with intervening marrow tissue. (B) Periosteal layers (arrows) surrounding the diaphysis. (C, D) Distal diaphyseal bone matrix containing osteocytes (OC), osteoblasts (OB), and osteoclasts (Ocl). (E) Distal diaphysis

showing cup-shaped trabeculae (BT) near the epiphyseal plate. (F) Ossification zone (large arrowhead) adjacent to cartilage zone (small arrowhead), with hypertrophic chondrocytes near calcified cartilage (arrow). H&E staining. Magnification: (A, B, E ×40), (C, D, F ×100). Data represent mean ± SD (n = 10 per group).

3.1.4. Histology of femur of the experimental group at day 14 of incubation

The paracentral region of the femur shaft in the experimental group was completely occupied by bone trabeculae, similar to the control group at day 14 of incubation. However, the bone marrow spaces adjacent to the proximo-distal diaphysis were markedly enlarged with discontinuously scattered trabeculae (Figure 4A, B). Hematoxylin and eosin staining revealed two trabecular patterns within the paracentral diaphysis: pink-stained trabeculae containing bone matrix with osteocytes within lacunae (Figure 4C), and dark-stained trabeculae appearing as variable-sized, hazy violet patches (Figure 4D). The latter showed condensed osteocyte nuclei with loss of cellular boundaries, while numerous osteoclasts surrounded both trabecular types (Figure 4E).

Comparison between the control (Figure 2A) and experimental groups demonstrated progressive enlargement of the medullary cavity in the experimental group, indicating active bone resorption. In addition, collar bone formation beneath the periosteum was observed only in the experimental group (Figure 4F).

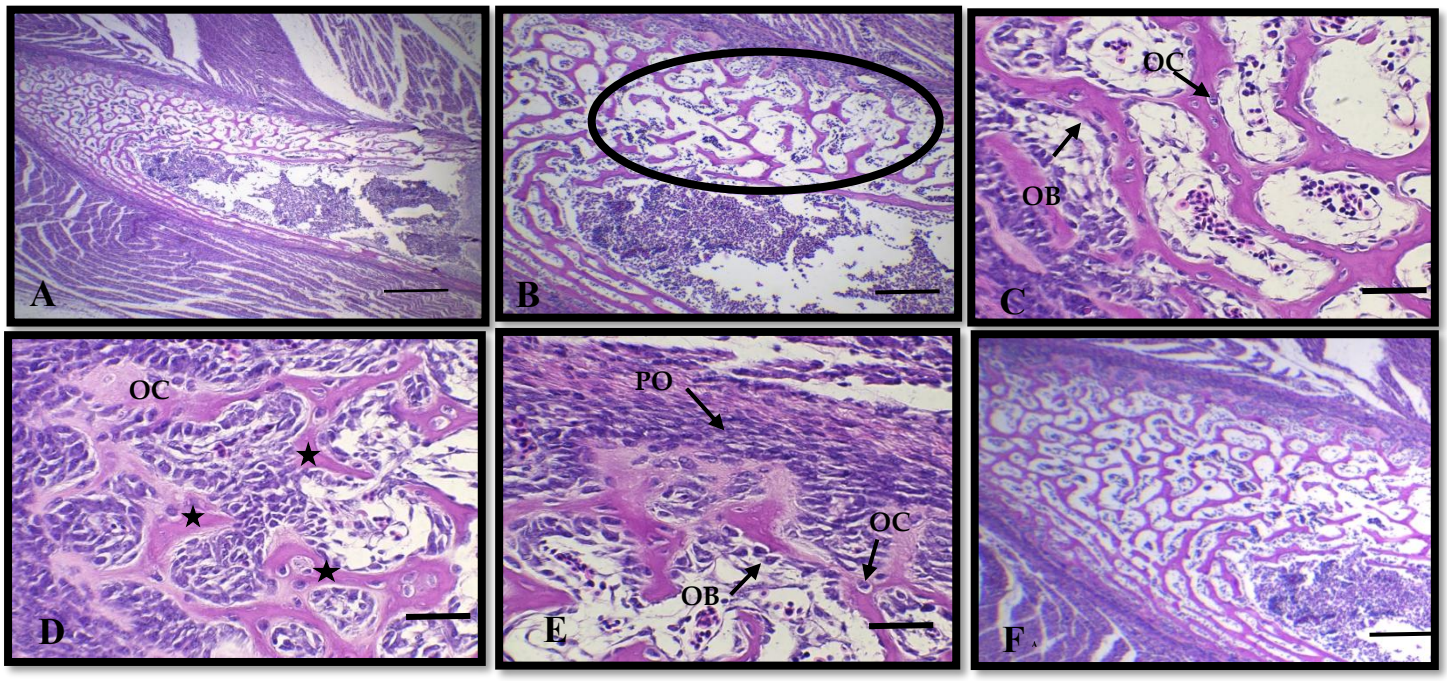


Figure (4): Sagittal section of femur in experimental chick embryo at day 14 of incubation. (A) Spongy appearance of femoral shaft. (B) Enlarged bone marrow spaces with discontinuous trabeculae. (C, D) Bone matrix containing osteocytes within lacunae (arrow) and dark-stained trabeculae (star). (E) Bone collar formation beneath periosteum (PO) with osteoblasts (OB) and osteocytes (OC) within bone matrix. (F) Widening of medullary cavity. H&E staining. Magnification: A, F ×40; B ×100; C–E ×400. Data represent mean ± SD (n = 10 per group).

3.2. Histochemical labeling of the developing femur

The immunohistochemical markers used in this study were associated with the onset of mineralization after days 13 and 14 of incubation. These markers were applied to evaluate the effects of calcium carbonate nanoparticles on bone cell differentiation, activity, and mineralization. They targeted bone-related proteins in the developing chick femur to assess differences in mineralization between control and experimental groups. Accordingly, the immunohistochemical evaluation focused on marker expression in the diaphyseal region of the femur.

3.2.1.1. Control group

High-power immunohistochemical examination showed brownish osteocalcin labeling surrounding many bony trabeculae. Brown-stained patches were also observed within the purple-stained trabeculae, while the remaining diaphyseal tissues showed no osteocalcin immunolabeling (Figure 5A).

3.2.1.2. Experimental group at day 13

The immunohistochemical brownish labeling surrounding the bony trabeculae was extensively distributed within the developing trabeculae of the femoral diaphysis in the experimental group. This labeling appeared subjectively darker than that observed in the control group sections.

The purple-stained bony trabeculae in the experimental group showed mottled light brown cloudiness, with numerous dark brown stained patches frequently observed within the trabeculae (Figure 5B).

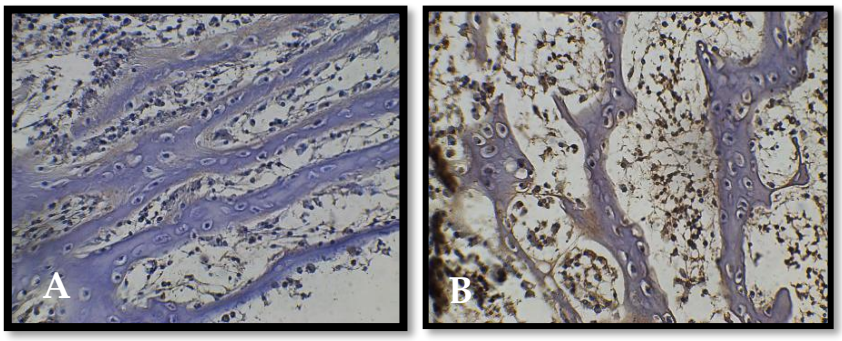


Figure (5): Immunohistochemical localization of osteocalcin in femoral diaphysis at day 13. (A) Control group showing osteocalcin immunolabeling surrounding bony trabeculae with brown-positive areas within trabecular matrix. (B) Experimental group showing extensive osteocalcin immunolabeling around developing bony trabeculae. Magnification: ×400.

3.2.1.3. Aperio Image Scope analysis

Immunohistochemical analysis was performed to evaluate osteocalcin expression in the femoral diaphysis of the control and experimental groups at day 13. The mean positive pixel area in the control group was 0.15 ± 0.028 (SD), significantly lower than that of the experimental group (0.32 ± 0.045; $p < 0.05$) (Table 1).

In the control group, osteocalcin immunolabeling appeared as brown staining surrounding the bony trabeculae, whereas the experimental group showed denser staining

within the trabeculae (Figure 6). These findings indicate increased osteocalcin expression and enhanced osteogenic activity in the experimental group following treatment.

Table 1. Mean positive pixel count of osteocalcin immunohistochemical labeling in the femoral diaphysis at day 13 (Aperio ImageScope Analysis)

	13 day		
Osteocalcin	**Control Mean±STD**	**Experimental Mean±STD**	**P-value**
	0.15±0.028	**0.32±0.030**	**0.0001***

* Significant at $p < 0.05$ and highly significant at $p \leq 0.0001$ using the independent t-test between control and experimental groups at day 13.

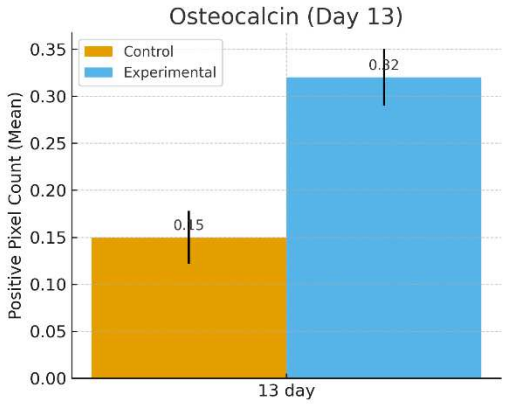


Figure (6): The statistical analysis of mean grey values was obtained to evaluate the osteocalcin immunohistochemical reaction in the diaphysis of the femur at day 13. Bars show mean positive pixel count ± SD (n = 10 per group).

3.2.2. Osteocalcin Labeling of Femurs at Day 14

3.2.2.1. Control Group

The osteocalcin labeling pattern in the developing trabeculae of the control group at day 14 resembled that observed in the experimental group at day 13. The central diaphysis showed light brown immunoreactivity mixed with the purple hue of the bony trabeculae, whereas the peripheral diaphysis exhibited stronger brown staining (Figure 7A).

3.2.2.2. Experimental Group

Both the central and peripheral trabeculae of the femoral diaphysis showed a similar pattern of osteocalcin labeling, characterized by light brown immunoreactivity mixed with the purple hue of the bony trabeculae (Figure 7 B).

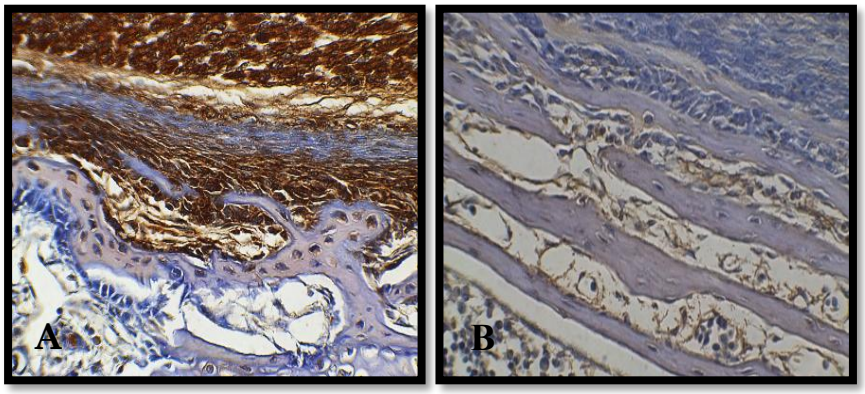


Figure (7): (A) Osteocalcin immunolabeling in femoral diaphysis (control, day 14) showing brown reactivity within central trabeculae and prominent peripheral staining. (B) Experimental group (day 14) shows regular brown osteocalcin staining mixed with the purple bone matrix, with light brown reactivity within trabeculae. ×400.

Table 2. Mean positive pixel count of osteocalcin immunohistochemical labeling in femur diaphysis at day 14 (Aperio ImageScope analysis).

	14 day		
Osteocalcin	**Control Mean±STD**	**Experimental Mean±STD**	**P-value**
	0.24±0.025	**0.13±0.015**	**0.0001***

*** Significant at $p < 0.05$ and highly significant at $p \leq 0.0001$ using the independent t-test between control and experimental groups at day 14.**

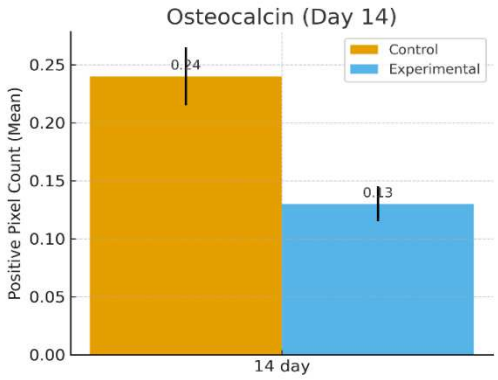


Figure (8): Statistical analysis of mean positive pixel count showing osteocalcin immunohistochemical expression in femoral diaphysis at day 14. Data are presented as mean ± SD (n = 10 per group).

3.3. Sialoprotein labeling of femurs of the day 13

3.3.1. Control group

Sialoprotein immunohistochemical labelling appeared as brown staining at the periphery of bony trabeculae, with positive reactivity also observed within many trabecular areas. Cells surrounding the trabeculae showed positive expression, including osteoprogenitor-like cells (spindle-shaped with flattened nuclei) and large mononucleated cells. Some of the large positively stained cells exhibited osteoclast-like features (Figure 9A).

3.3.2. Experimental group (day 13)

Diffuse brown immunohistochemical labelling was observed in developing bony trabeculae at the femoral diaphysis. The trabeculae showed a light brown matrix, and numerous surrounding cells also demonstrated positive sialoprotein reactivity (Figure 9B).

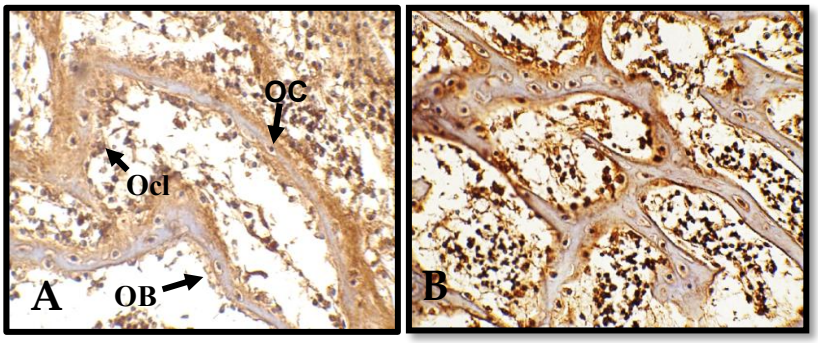


Figure 9. Sialoprotein immunolabeling in femoral diaphysis at day 13. (A) Control group showing brown staining at trabecular periphery with osteoclasts (Ocl), spindle-shaped osteoblasts (OB), and osteocytes (OC) within lacunae. (B) Experimental group showing diffuse brown sialoprotein staining in developing trabeculae with light brown matrix. Magnification: ×400.

3.3. Aperio ImageScope Analysis

The mean positive pixel count in femur diaphysis trabeculae showed a statistically significant difference between groups (Figures 10). The control group recorded a mean value of 0.78 ± 0.047 SD, while the experimental group showed a slightly higher value of 0.84 ± 0.024 SD (Table 3).

Table (3): Mean positive pixel count of sialoprotein immunolabeling in femur diaphysis (day 13) in control and experimental groups (Aperio ImageScope analysis).

	13 day		
	Control Mean±STD	**Experimental Mean±STD**	**P-value**
Sialoprotein	**0.78±0.047**	**0.84±0.024**	**0.0001***

* Significant at $p < 0.05$ and highly significant at $p \leq 0.0001$ using the independent t-test between control and experimental groups at day 13.

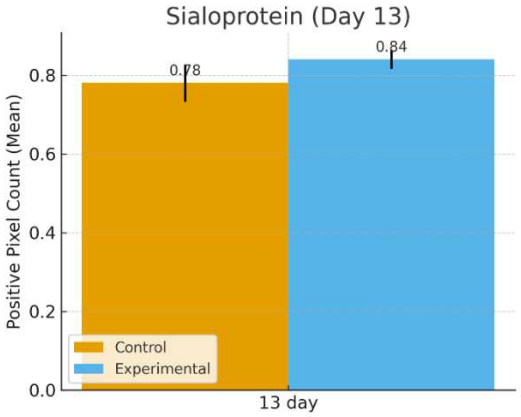


Figure (10): Statistical analysis of positive pixel evaluation for sialoprotein immunohistochemical expression in femur diaphysis at day 13. Data are presented as mean ± SD (n = 10 per group).

3.3.4. Sialoprotein Labeling of Femurs (Day 14)

3.3.4.1. Control group (Day 14):

Light brown reactivity was disclosed in developing bony trabeculae in the femur diaphysis with sialoprotein immunolabeling, and many cells surrounding the trabeculae also showed positive immunoreactivity (Figure 11A).

3.3.4.2. Experimental group (Day 14):

The diaphyseal trabeculae and many surrounding cells showed brownish sialoprotein labeling with light brown matrix reactivity (Figure 11B).

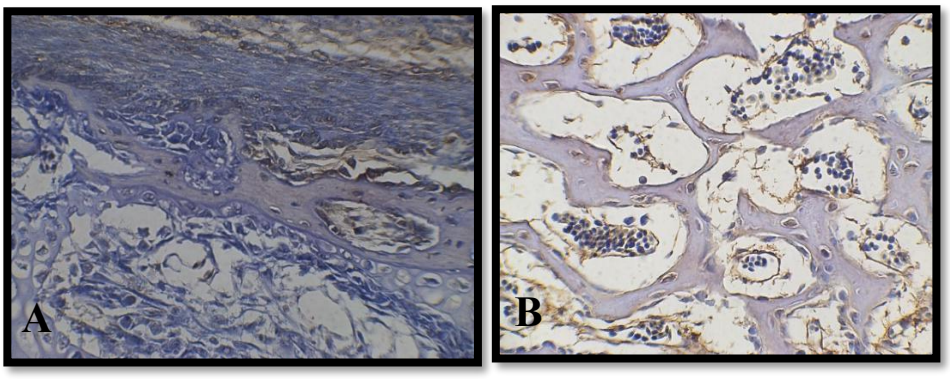


Figure (11): Sialoprotein immunohistochemical staining in femoral diaphysis at day 14. (A) Control group showing light brown positivity in cells adjacent to bony trabeculae. (B) Experimental group showing brown labeling with a light brown hue.

3.4.5. Aperio Image Scope Analysis

The mean level of measured positive pixels in the trabecular bone of the femoral diaphysis revealed statistically nonsignificant difference between the control and experimental groups (Figure 12). The mean value was (0.3 ± 0.045 STD) in the control group and (0.31 ± 0.047 STD) in the experimental group, showing a slight increase in the experimental group ($p \geqslant 0.051$) (Table 4).

Table (4): Mean positive pixel count of sialoprotein immunolabeling in femur diaphysis (day 14) in control and experimental groups (Aperio ImageScope analysis).

	14 day		
Sialoprotein	**Control Mean±STD**	**Experimental Mean±STD**	**P-value**
	0.3±0.045	**0.31±0.047**	**0.051**

* Significant at $p < 0.05$ and highly significant at $p \leq 0.0001$ using the independent t-test between control and experimental groups at day 14.

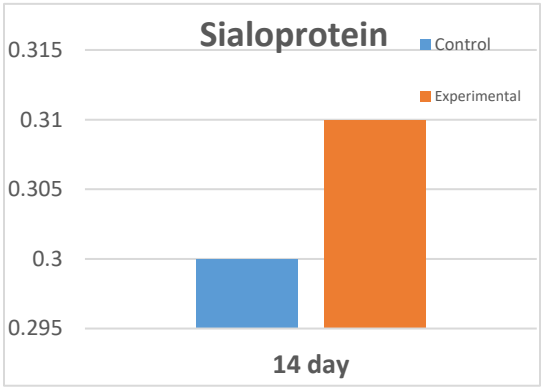


Figure (12): Statistical analysis of positive pixel evaluation for sialoprotein immunohistochemical expression in femur diaphysis at day 14. Data are presented as mean ± SD (n = 10 per group).

3.4. Radiographic description of the developing femur

Radiographs of the lower limbs from embryos of both groups indicated hazy boundaries of the developing femur in the control group, especially at earlier stages. Relative haziness was observed in the control group compared with the experimental group at the same developmental stages (Figures 13–18).

However, the marginal border separating the thigh soft tissues and femur bone was sufficiently delineated to enable selection of a constant rectangular region at the middle diaphysis

for ImageJ evaluation of mean grey values. Similar rectangles were selected at the proximo-distal diaphysis to evaluate mean grey values using ImageJ software.

Statistical analysis of mean grey values from radiographic images of the developing femur in chick embryos of the control and experimental groups, evaluated by ImageJ software, revealed significant variations across successive embryonic stages (Figure 19).

At day 13, the femoral diaphysis of the experimental group demonstrated a highly significant increase in mean grey values (677.5 ± 17.8 SD) compared with the control group ($P < 0.0001$). Conversely, at day 14 displayed a highly significant decrease in mean grey values (603.9 ± 14.9 SD) in the experimental group relative to the control group ($P < 0.0001$).

Moreover, statistical assessment indicated gradual increase in mean grey values in the experimental group during developmental days 15–18 related with the control group at the same stages (Table 5).

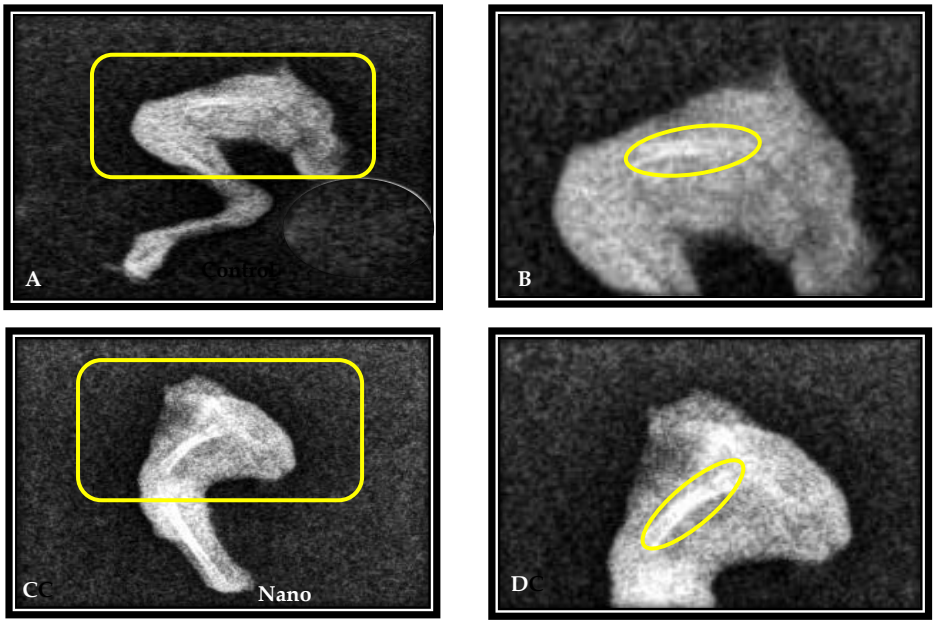


Figure (13): Radiographic images of the developing lower limbs (femur) at day 13 from control (A&B) and experimental (C&D) groups with high magnification.

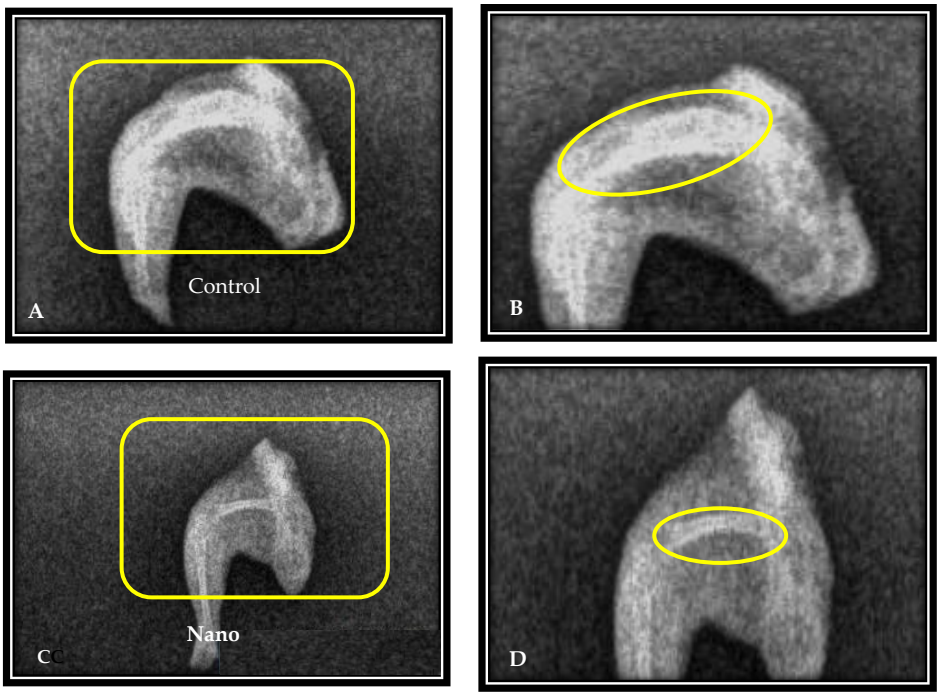


Figure (14): Radiographic images of the developing lower limbs (femur) at day 14 from control (A&B) and experimental (C&D) groups with high magnification.

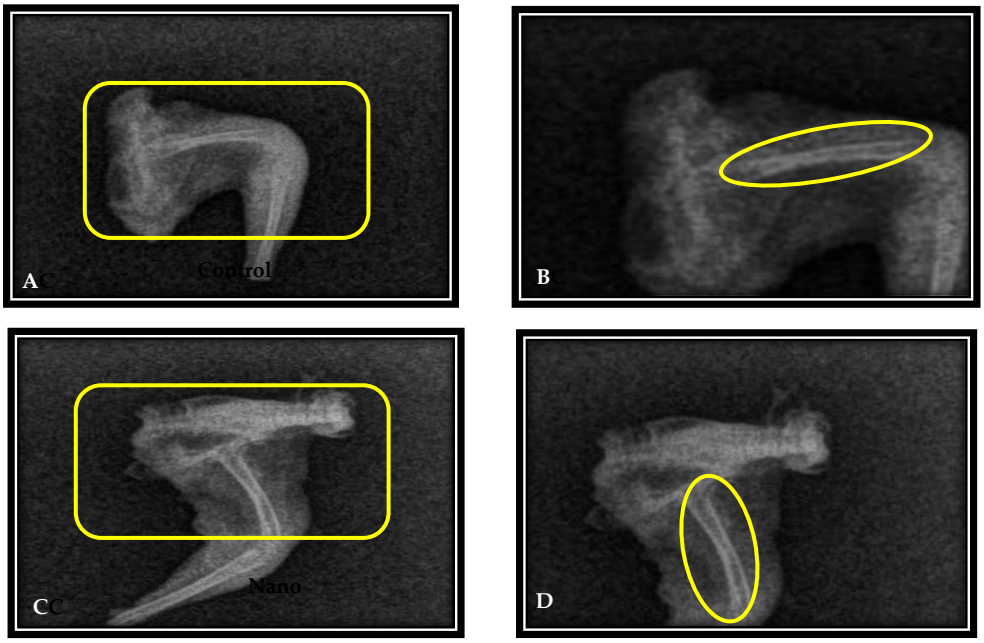


Figure (15): Radiographic images of the developing lower limbs (femur) at day 15 from control (A&B) and experimental (C&D) groups with high magnification.

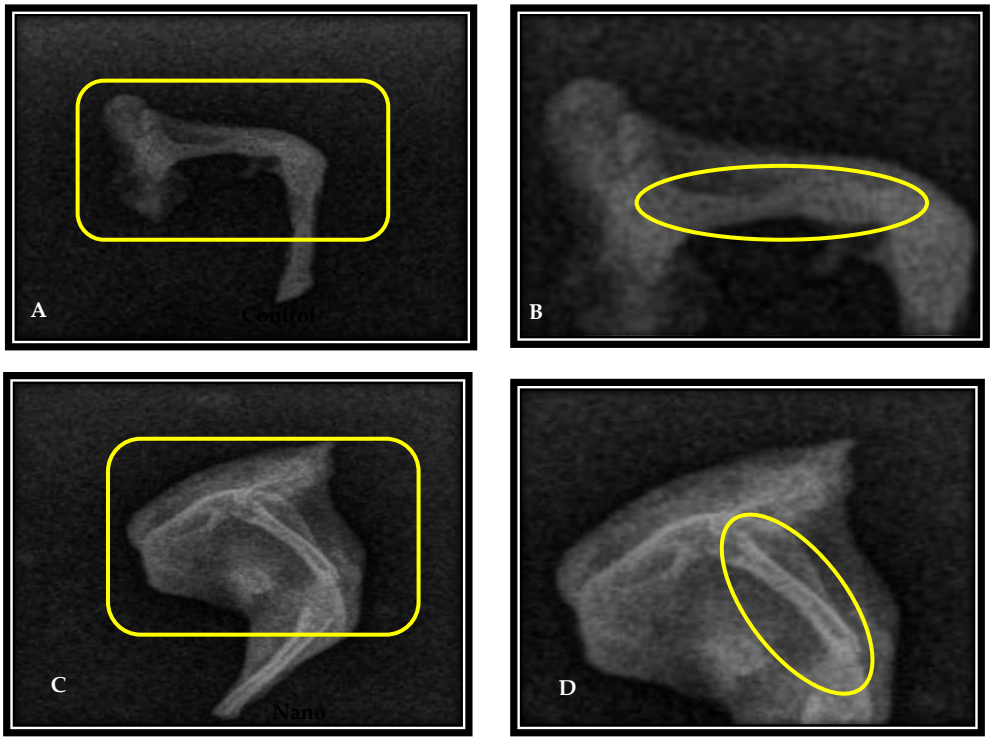


Figure (16): Radiographic images of the developing lower limbs (femur) at day 16 from control (A&B) and experimental (C&D) groups with high magnification.

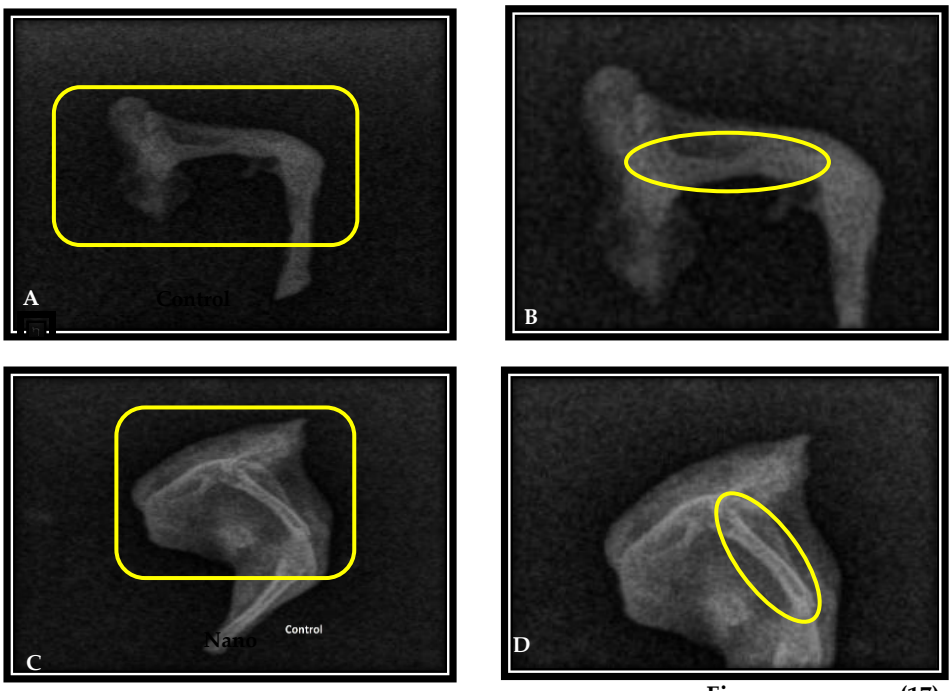


Figure (17): Radiographic images of the developing lower limbs (femur) at day 17 from control (A&B) and experimental (C&D) groups with high magnification.

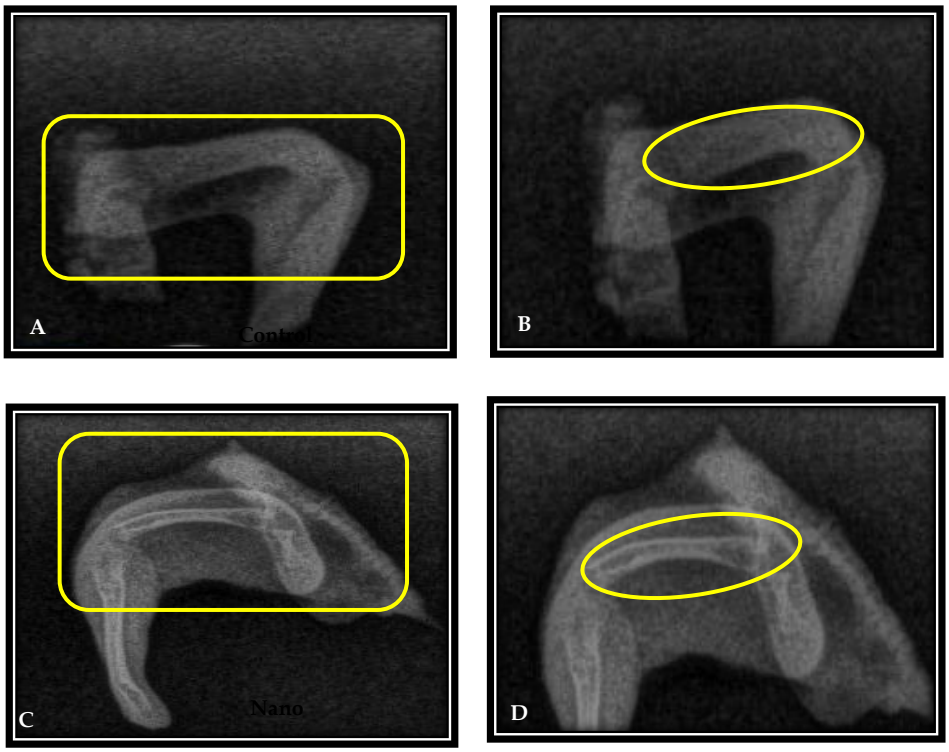


Figure (18): Radiographic images of the developing lower limbs (femur) at day 18 from control (A&B) and experimental (C&D) groups with high magnification.

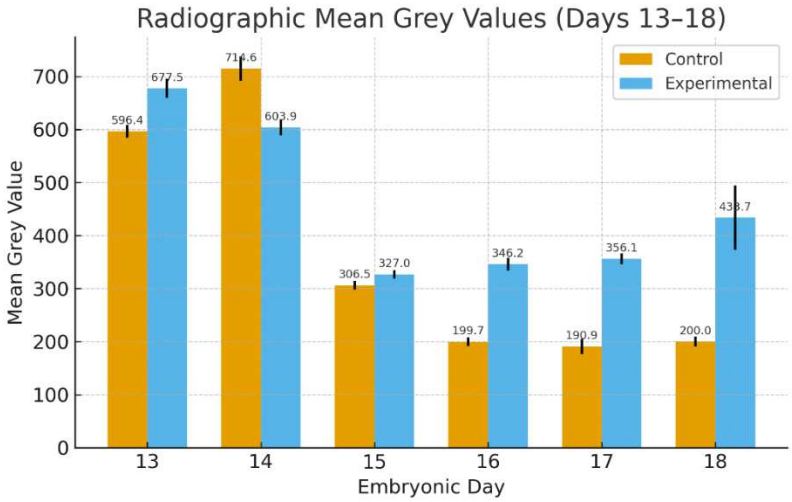


Figure (19): Statistical assessment of positive pixel evaluation for radiological evaluation of the femoral development in chick embryos of control and experimental groups from days 13–18. Bars represent mean ± SD (n = 10 per group per day).

Table (5): Mean Values of Radiological Data for Developing Femurs in Chick Embryos: Comparison Between Control and Experimental Groups from Day 13 to Day 18.

			95% Confidence Interval of the				
Groups	**Control**	**Experimental**	**Lower**	**Upper**	**F-statistic**	**Degree of Freedom**	**P-value**
Day 13	**596.4±12.1**	**677.5±17.8**	**95.57**	**66.68**	**11.91**	**15.85**	**<0.0001***
Day 14	**714.6±22.6**	**603.9±14.9**	**94.41**	**130.91**	**13.11**	**15.57**	**<0.0001***
Day 15	**306.5±8.8**	**327±7.6**	**28.33**	**12.77**	**5.56**	**17.59**	**<0.0001***
Day 16	**199.7±7.9**	**346.2±12**	**156.27**	**136.88**	**32.12**	**15.53**	**<0.0001***
Day 17	**190.9±13.7**	**356.1±10.6**	**176.80**	**153.64**	**30.11**	**16.94**	**<0.0001***
Day 18	**200±9.2**	**433.7±60.5**	**274.37**	**193.06**	**12.07**	**18**	**<0.0001***

* Significant at $p < 0.05$ and highly significant at $p \leq 0.0001$ using the independent t-test between control and experimental groups at day 13-18.

4. Discussion

4.1. Evidence of the effect of CCN on osteogenesis of femur

The results of this study showed a developmentally advanced histological configuration in the femoral diaphysis induced by CCN. These findings support previous conclusions [23] regarding the role of CCN in modifying molecular responses during embryogenesis and enhancing bone mineralization. The observed histological features in the experimental group suggest that CCN accelerates chick embryo femoral osteogenesis at day 13, shifting development toward a more advanced stage, approximately resembling day 14. This effect may be explained by the proposed role of CCN in regulating osteogenic differentiation [23].

Calcium ions have been proposed as coupling factors between osteoblasts and osteoclasts, influencing osteogenic differentiation through calcium-related signaling pathways and regulation of calcium-dependent proteins. This supports the observed increase in osteogenic activity in the femoral diaphysis in this study.

The results also indicate that CCN does not adversely affect embryonic chondrogenesis or osteogenesis. Previous studies on mesenchymal stem cells showed that nanoparticle properties such as composition, size, shape, surface charge, and surface chemistry influence cellular responses [24]. Nanoparticle cytotoxicity is generally dose-dependent and cell-type specific, and related to particle–cell interactions [25,26]. Although cytotoxicity of CCN has been reported under certain conditions [27,28], the present CCN formulation appears non-cytotoxic. Overall, the findings agree with reports describing the good biocompatibility and low toxicity of CCN in developing tissues [29,30].

4.2. Histological changes of femur in the control and experimental groups

The morphological description of the femur using H&E staining was satisfactory. The staining pattern agrees with previous reports [31], which noted that both bone and soft tissues appear eosinophilic, making differentiation difficult.

In the day 13 control group, increased trabecular thickness in the paracentral diaphysis resembled findings in mice at comparable developmental stages [32].

The proximo-distal regions of the femoral diaphysis in day 13 experimental embryos showed more advanced maturation compared with controls, consistent with previous descriptions [33,34].

These findings support reports [35,36] on endochondral ossification in long bones, which depends on vascular supply for osteoblast and osteoclast progenitors. The vascular pattern associated with trabecular formation showed numerous osteoprogenitor cells, osteoblasts, and osteoclasts in femoral sections [37].

Previous studies [37] reported that White Leghorn chick embryos at days 13–15 exhibit a calcified trabecular network in the mid-diaphysis with osteoblasts on trabecular surfaces, supporting the present results. This histological framework may also support immunohistochemical evaluation of bone formation and mineralization markers [38].

It was also reported [37] that after day 15, femurs show enlarged marrow cavities surrounded by cortical bone with loss of trabeculae due to osteoclastic resorption. Bone resorption involves mineral dissolution and organic matrix degradation [39]. These findings support the enlarged marrow cavities observed here as part of progressive mid-diaphyseal development.

4.3. Osteocalcin and sialoprotein inflections after exposure of the femoral diaphyseal bone trabeculae to CCN

The antibodies used in this study detected histochemical changes of the bone matrix proteins osteocalcin and sialoprotein, which are expressed and incorporated into the collagenous matrix of bony trabeculae during sequential stages of bone maturation [40]. The findings showed increased osteocalcin and sialoprotein expression in the femoral trabeculae at day 13 after CCN exposure, supporting the histological evidence of accelerated bone maturation induced by CCN.

4.4. Appraisal of osteocalcin changes in the femoral diaphyseal bone trabeculae:

Osteocalcin is a protein specifically expressed in osteoblasts [41–44]. Since hydroxyapatite crystals form the mineral component of bone, carboxylated osteocalcin was reported to inhibit hydroxyapatite growth during mineralization [42–47]. It also acts as a chemoattractant for osteoclast precursors [47]. Osteocalcin has been described as a negative regulator of bone formation and resorption through inhibition of osteoblast function and osteoclastogenesis [48,49].

Therefore, the increased osteocalcin expression observed in the bony trabeculae after CCN exposure at day 13 may represent a physiological response associated with temporary arrest of trabecular formation during this developmental stage. This inhibition may indicate advanced maturation of femoral diaphyseal trabeculae, followed by trabecular degradation by osteoclasts in the mid-diaphysis, as observed histologically in this study.

The increased osteocalcin expression at day 13 may also reflect inhibition of osteoclastogenesis before active osteoclastic degradation of trabeculae during progressive bone maturation.

At day 14, osteocalcin expression markedly decreased in the bony trabeculae of the experimental group. This reduction may reflect the physiological activation of osteoclastogenesis and bone resorption in the mid-diaphysis. The decrease in osteocalcin expression after CCN exposure may also indicate reduced osteoblastic expression of this protein in the trabeculae of this region.

4.5. Appraisal of sialoprotein changes in the femoral diaphyseal bone trabeculae

Previous studies reported that hypertrophic chondrocytes and osteoblasts express sialoprotein during the onset of bone mineralization [50–53]. Sialoprotein belongs to the Small Integrin-Binding Ligand N-linked Glycoprotein (SIBLING) family [53] and forms part of the non-collagenous extracellular matrix proteins [54,55].

Sialoprotein-mediated cell-surface receptor activation and intracellular signaling were reported to regulate osteoblast and osteoclast activity [56]. Increased sialoprotein expression enhances matrix mineralization by osteoblasts, while osteoclasts also express and interact with this protein [57,58]. Sialoprotein is considered important in osteoclastogenesis [57,59] and bone resorption [60].

These findings support the interpretation of the present results. The significant increase in sialoprotein expression within the bony trabeculae of the femoral mid-diaphysis at day 13 after CCN exposure may indicate osteoblastic overexpression associated with the onset of mineralization and its regulation. The non-significant increase observed at day 14 may be related to active osteoclastic function.

4.6. Radiographic changes of femur in the control and experimental groups

The statistical analysis of mean grey values from femoral radiographs after CCN exposure showed a significant increase at day 13 in the femoral diaphysis of the experimental group. This finding supports the suggestion that the increased trabecular osteocalcin and sialoprotein expression at this stage reflects accelerated bone maturation induced by CCN.
Similarly, the significant decrease in mean grey values at day 14 in the experimental group corresponded with the reduction in trabecular osteocalcin expression, which may reflect the physiological activation of bone resorption and osteoclastogenesis in the mid-diaphysis.

Although histological and immunohistochemical assessments in this study did not extend beyond day 14, the radiological evaluation at days 15–18 may be interpreted according to previous reports on cortical bone development. The progressive increase in mean grey values during these stages may indicate enhanced cortical osteogenesis and mineralization induced by CCN through modification of molecular responses during embryogenesis. These findings also support previous suggestions [23] regarding possible long-term effects of CCN exposure on bone quality. Cortical bone was previously described as initially consisting of immature woven bone that progressively calcifies and matures during later developmental stages. Therefore, CCN exposure may promote progressive bone maturation and osteogenic differentiation throughout femoral development.

Several techniques have been used to evaluate bone mineralization, including quantitative computed tomography [61,62] and dual-energy X-ray absorptiometry [63]. In digitally processed radiographs analyzed by ImageJ software, grey value measurements represent a simple method related to X-ray absorption [64].

ImageJ software is freely available, easily integrated into research analysis, and can be modified according to user requirements [65]. It has been used as a semi-automated tool for bone structure analysis, evaluation of bone anabolic activity, and osteoporosis research [66]. Many recent studies in biology and health sciences have applied ImageJ for digital image analysis because it allows image display, editing, analysis, and processing in DICOM and JPEG formats [67]. ImageJ was also validated for assessing trabecular bone density in radiographic images [64,68]. These applications support the conclusions of the present study regarding the effects of CCN on femoral development.

Conclusions:

Calcium carbonate nanoparticles (CCN) appear to play a regulatory role in osteogenic differentiation, likely through modulation of calcium ion-related signaling pathways and the expression of calcium-dependent proteins, which are key mediators between osteoblasts and osteoclasts.

The immunohistochemical labeling of the bony trabeculae with both osteocalcin and sialoprotein in the femur diaphysis at day 13, influenced by CCN, showed significantly increased values. The data indicate that CCN may contribute to the regulation of bone development and osteoblast activity.

Radiographic analysis corroborated the histological and immunohistochemical results. The increased mean grey value in the femoral diaphysis on day 13, following CCN exposure, supports the occurrence of enhanced trabecular mineralization as a developmental effect of CCN, which contributes to the progression of bone maturation. The decrease in mean grey values observed in the femurs of the experimental group on day 14 reflects the physiological process of diaphyseal bone resorption.

Data Availability

The datasets generated and/or analyzed during the current study are available from the corresponding author on reasonable request.

Authors' contributions:

Hayder J. Kadhim designed the study.

Lamyaa hadi worked the experimental laboratory work.

Fatma Ayadi the tunisesia arranged the documentation of the results.

All authors read and approved the final version of the manuscript.

Funding

No external funding sources.

Declaration of Competing Interest:

The authors declare that they have no conflicts of interest to dis- close.

Acknowledgments:

We would like to thank all the staff members of the college of medicine Al-Nahrain University for the support provided in the study. My sincere thanking to Prof. Dr. Asmaa Hadi Mohammed and Assist. Prof. Dr. Marwa A. Hassan for deep help.

References:

ABDULHUSSIEN, I. A., MUBARAK, H. J. & HAMID, M. K. 2020. In ovo influence of silver nanoparticles on the developmental stage specific abnormalities in chick embryo. *EurAsian Journal of Biosciences,* 14.

AFROZE, S. N., RAMULU, S., RAO, G. V., TANEERU, S., BASHAMALLA, R. & VADLA, P. 2018. Demystifying the nature of hard tissues in odontogenic tumors using Modified Gallego's stain: A preliminary study. Journal of Oral and Maxillofacial Pathology, 22, 448.

BAILER, W. 2006. Writing ImageJ plugins—a tutorial. *Upper Austria University of Applied Sciences, Austria. Available on:* http://www. *gm. fh-koeln. de/~ konen/WPF-BV/tutorial-ImageJ_V1,* 71.

BIANCO, P., RIMINUCCI, M., SILVESTRINI, G., BONUCCI, E., TERMINE, J., FISHER, L. & ROBEY, P. G. 1993. Localization of bone sialoprotein (BSP) to Golgi and post-Golgi secretory structures in osteoblasts and to discrete sites in early bone matrix. Journal of Histochemistry & Cytochemistry, 41, 193-203.

BOSKEY, A. L. & ROBEY, P. G. 2013. The regulatory role of matrix proteins in mineralization of bone. Osteoporosis. Elsevier.

BOSKEY, A. L., WIANS, F. & HAUSCHKA, P. V. 1985. The effect of osteocalcin on in vitro lipid-induced hydroxyapatite formation and seeded hydroxyapatite growth. Calcified tissue international, 37, 57-62.

BOULEFTOUR, W., JUIGNET, L., BOUET, G., GRANITO, R. N., VANDEN-BOSSCHE, A., LAROCHE, N., AUBIN, J. E., LAFAGE-PROUST, M.-H., VICO, L. & MALAVAL, L. 2016. The role of the SIBLING, Bone Sialoprotein in skeletal biology—Contribution of mouse experimental genetics. Matrix biology, 52, 60-77.

CHANG, A., BREELAND, G., BLACK, A. C. & HUBBARD, J. B. 2023. Anatomy, Bony Pelvis and Lower Limb: Femur. StatPearls [Internet]. StatPearls Publishing.

CHAVEZ, M., TAN, M., KOLLI, T., ZACHARIADOU, C., FARAH, F., MOHAMED, F., CHU, E. & FOSTER, B. 2023. Bone sialoprotein is critical for alveolar bone healing in mice. Journal of Dental Research, 102, 187-196.

CHEN, J., SHAPIRO, H. S., WRANA, J. L., REIMERS, S., HEERSCHE, J. N. & SODEK, J. 1991. Localization of bone sialoprotein (BSP) expression to sites of mineralized tissue formation in fetal rat tissues by in situ hybridization. Matrix, 11, 133-143.

COOPER, K. L. 1989. Radiology of metabolic bone disease. *Endocrinology and metabolism clinics of North America,* 18**,** 955-976.

DECUYPERE, E., TONA, K., BRUGGEMAN, V. & BAMELIS, F. 2001. The day-old chick: a crucial hinge between breeders and broilers. World's Poultry Science Journal, 57, 127-138.

DHAWAN, V., KAPOOR, K., SHARMA, M., SINGH, B., SEHGAL, A. & KOCHHAR, S. 2014. Histological study of the developing human femur. Eur J Anat, 18, 273-282.

DUCY, P. 2011. The role of osteocalcin in the endocrine cross-talk between bone remodelling and energy metabolism. Diabetologia, 54, 1291-1297.

DUCY, P., DESBOIS, C., BOYCE, B., PINERO, G., STORY, B., DUNSTAN, C., SMITH, E., BONADIO, J., GOLDSTEIN, S. & GUNDBERG, C. 1996. Increased bone formation in osteocalcin-deficient mice. Nature, 382, 448-452.

FERNÁNDEZ-IGLESIAS, Á., FUENTE, R., GIL-PEÑA, H., ALONSO-DURÁN, L., SANTOS, F. & LÓPEZ, J. M. 2021. The formation of the epiphyseal bone plate occurs via combined endochondral and intramembranous-like ossification. International Journal of Molecular Sciences, 22, 900.

GERBER, H.-P. & FERRARA, N. 2000. Angiogenesis and bone growth. Trends in cardiovascular medicine, 10, 223-228.

GEIGER, M., BLEM, G. & LUDWIG, A. 2016. Evaluation of ImageJ for relative bone density measurement and clinical application. *Journal of Oral Health and Craniofacial Science,* 1**,** 012-021.

GOLDBERG, H. A. & HUNTER, G. K. 2012. Functional domains of bone sialoprotein. Phosphorylated extracellular matrix proteins of bone and dentin, 2, 266-282.

GOLDBERG, S. 2008. Mechanical/physical methods of cell disruption and tissue homogenization. 2D PAGE: Sample preparation and fractionation, 3-22.

GORDON, J. A., HUNTER, G. K. & GOLDBERG, H. A. 2008. Activation of the mitogen-activated protein kinase pathway by bone sialoprotein regulates osteoblast differentiation. Cells Tissues Organs, 189, 138-143.

GOWIN, W., SAPARIN, P. I., KURTHS, J. & FELSENBERG, D. 1998. Measures of complexity for cancellous bone. *Technology and Health Care,* 6**,** 373-390.

GWEN, M. R., FIRMAN, R. N. & PRAMANIK, F. 2020. Description of condyle trabecular bone density of hypertension patients evaluated from panoramic radiograph using software imageJ. *Journal of Dentomaxillofacial Science,* 5**,** 77-81.

HAUSCHKA, P. V., LIAN, J. B., COLE, D. & GUNDBERG, C. M. 1989. Osteocalcin and matrix Gla protein: vitamin K-dependent proteins in bone. Physiological reviews, 69, 990-1047.

HE, F., ZHANG, J., YANG, F., ZHU, J., TIAN, X. & CHEN, X. 2015. In vitro degradation and cell response of calcium carbonate composite ceramic in comparison with other synthetic bone substitute materials. Materials Science and Engineering: C, 50, 257-265.

HELFRICH, M. H., NESBITT, S. A., DOREY, E. L. & HORTON, M. A. 1992. Rat osteoclasts adhere to a wide range of RGD (Arg-Gly-Asp) peptide-containing proteins, including the bone sialoproteins and fibronectin, via a β3 integrin. Journal of Bone and Mineral Research, 7, 335-343.

HUANG, L.-H., SUN, X.-Y. & OUYANG, J.-M. 2019. Shape-dependent toxicity and mineralization of hydroxyapatite nanoparticles in A7R5 aortic smooth muscle cells. Scientific reports, 9, 18979.

HUANG, S., CHEN, J. C., HSU, C. W. & CHANG, W. H. 2009. Effects of nano calcium carbonate and nano calcium citrate on toxicity in ICR mice and on bone mineral density in an ovariectomized mice model. Nanotechnology, 20, 375102.

HOSSEINIAN, S. & AREFI, H. 2017. Photogrammetry in 3D modelling of human bone structures from radiographs. *The International Archives of the Photogrammetry, Remote Sensing and Spatial Information Sciences,* 42**,** 115-121.

JING, Y., JING, J., YE, L., LIU, X., HARRIS, S. E., HINTON, R. J. & FENG, J. Q. 2017. Chondrogenesis and osteogenesis are one continuous developmental and lineage defined biological process. Scientific reports, 7, 10020.

KACHI, M., SUGIYAMA, T. & KUSUHARA, S. 2008. Endochondral ossification of chick embryonic femora in vitro and on chorioallantoic membrane. The Journal of Poultry Science, 45, 51-56.

KHANAL, T. 2020. Rearing Mineral Nutrition and Housing Cage Type: Impact on Bone Quality in Pullets and Hens. University of Guelph.

KOMORI, T. 2020. What is the function of osteocalcin? Journal of oral biosciences, 62, 223-227.

KONG, X., XU, S., WANG, X., CUI, F. & YAO, J. 2012. Calcium carbonate microparticles used as a gene vector for delivering p53 gene into cancer cells. Journal of biomedical materials research Part A, 100, 2312-2318.

KOZHEMYAKINA, E., LASSAR, A. B. & ZELZER, E. 2015. A pathway to bone: signaling molecules and transcription factors involved in chondrocyte development and maturation. Development, 142, 817-831.

KRUG, R., BURGHARDT, A. J., MAJUMDAR, S. & LINK, T. M. 2010. High-resolution imaging techniques for the assessment of osteoporosis. *Radiologic Clinics,* 48**,** 601-621.

LAMMI, P., LAMMI, M., HYTTINEN, M., PANULA, H., KIVIRANTA, I. & HELMINEN, H. 2002. Site-specific immunostaining for type X collagen in noncalcified articular cartilage of canine stifle knee joint. Bone, 31, 690-696.

MALAVAL, L., WADE-GUÉYE, N. M., BOUDIFFA, M., FEI, J., ZIRNGIBL, R., CHEN, F., LAROCHE, N., ROUX, J.-P., BURT-PICHAT, B. & DUBOEUF, F. 2008. Bone sialoprotein plays a functional role in bone formation and osteoclastogenesis. The Journal of experimental medicine, 205, 1145-1153.

MATUSZEWSKI, A., ŁUKASIEWICZ, M., NIEMIEC, J., KAMASZEWSKI, M., JAWORSKI, S., DOMINO, M., JASIŃSKI, T., CHWALIBOG, A. & SAWOSZ, E. 2021. Calcium Carbonate nanoparticles—Toxicity and effect of in ovo inoculation on chicken embryo development, broiler performance and bone status. *Animals,* 11**,** 932.

MENANTEAU, J., NEUMAN, W. F. & NEUMAN, M. W. 1982. A study of bone proteins which can prevent hydroxyapatite formation. Metabolic Bone Disease and Related Research, 4, 157-162.

MESSINA, C., ALBANO, D., GITTO, S., TOFANELLI, L., BAZZOCCHI, A., ULIVIERI, F. M., GUGLIELMI, G. & SCONFIENZA, L. M. 2020. Body composition with dual energy X-ray absorptiometry: from basics to new tools. *Quantitative imaging in medicine and surgery,* 10**,** 1687.

MIURA, K., PAUL-GILLOTEAUX, P., TOSI, S. & COLOMBELLI, J. 2020. Workflows and components of bioimage analysis. *Bioimage Data Analysis Workflows***,** 1-7.

MIZOGUCHI, T. & ONO, N. 2020. The diverse origin of bone-forming osteoblasts. Journal of Bone and Mineral Research, 36, 1432-1447.

PANWAR, J., MATHEW, A. J., JINDAL, N. & DANDA, D. 2017. Utility of plain radiographs in metabolic bone disease–a case-based pictorial review from a tertiary centre. *Polish Journal of Radiology,* 82**,** 333.

PATEL, A. A., RAMANATHAN, R., KUBAN, J. & WILLIS, M. H. 2015. Imaging findings and evaluation of metabolic bone disease. *Advances in Radiology,* 2015**,** 812794.

PECHAK, D., KUJAWA, M. & CAPLAN, A. 1986. Morphology of bone development and bone remodeling in embryonic chick limbs. Bone, 7, 459-472.

PRICE, P. A., OTSUKA, A., POSER, J. W., KRISTAPONIS, J. & RAMAN, N. 1976. Characterization of a gamma-carboxyglutamic acid-containing protein from bone. Proceedings of the National Academy of Sciences, 73, 1447-1451.

PV, H. 1975. Direct identification of the calcium-binding amino acid, gamma-carboxyglutamate, in mineralized tissue. Proc Natl Acad Sci, 72, 3925-3929.

RETNOAJI, B., WULANDARI, R., NURHIDAYAT, L. & DARYONO, B. 2016. Osteogenesis study of hybrids of Indonesia's native chicken Pelung (Gallus gallus domesticus) with Broiler (Gallus gallus domesticus). Asian Journal of Animal and Veterinary Advances, 11, 498-504.

ROMBERG, R. W., WERNESS, P. G., RIGGS, B. L. & MANN, K. G. 1986. Inhibition of hydroxyapatite-crystal growth by bone-specific and other calcium-binding proteins. Biochemistry, 25, 1176-1180.

ROSS, F. P., CHAPPEL, J., ALVAREZ, J., SANDER, D., BUTLER, W., FARACH-CARSON, M., MINTZ, K., ROBEY, P. G., TEITELBAUM, S. & CHERESH, D. 1993. Interactions between the bone matrix proteins osteopontin and bone sialoprotein and the osteoclast integrin alpha v beta 3 potentiate bone resorption. Journal of Biological Chemistry, 268, 9901-9907.

SAKAMOTO, A., CHEN, M., NAKAMURA, T., XIE, T., KARSENTY, G. & WEINSTEIN, L. S. 2005. Deficiency of the G-protein α-subunit Gsα in osteoblasts leads to differential effects on trabecular and cortical bone. Journal of Biological Chemistry, 280, 21369-21375.

SEIBEL, M. J. 2005. Biochemical markers of bone turnover part I: biochemistry and variability. The Clinical biochemist. Reviews/Australian Association of Clinical Biochemists., 26, 97.

SITZMANN, F. 1993. Wann sind zur Sicherung von Diagnose und Therapie Röntgenaufnahmen nötig. *Stellungnahme,* 2**,** 147-148.

ŠROMOVÁ, V., SOBOLA, D. & KASPAR, P. 2023. A brief review of bone cell function and importance. Cells, 12, 2576.

SOBH, M. M., ABDALBARY, M., ELNAGAR, S., NAGY, E., ELSHABRAWY, N., ABDELSALAM, M., ASADIPOOYA, K. & EL-HUSSEINI, A. 2022. Secondary osteoporosis and metabolic bone diseases. *Journal of Clinical Medicine,* 11**,** 2382.

SÖZEN, T., ÖZıŞıK, L. & BAŞARAN, N. Ç. 2017. An overview and management of osteoporosis. *European journal of rheumatology,* 4**,** 46.

SUVARNA, K. S., LAYTON, C. & BANCROFT, J. D. 2018. Bancroft's theory and practice of histological techniques, Elsevier health sciences.

SUZUKI, Y., MATSUBAYASHI, J., JI, X., YAMADA, S., YONEYAMA, A., IMAI, H., MATSUDA, T., AOYAMA, T. & TAKAKUWA, T. 2019. Morphogenesis of the femur at different stages of normal human development. PLoS One, 14, e0221569.

SUVARNA, K. S., LAYTON, C. & BANCROFT, J. D. 2018a. *Bancroft's theory and practice of histological techniques*, Elsevier health sciences.

SUVARNA, K. S., LAYTON, C. & BANCROFT, J. D. 2018b. *Bancroft's Theory and Practice of Histological Techniques E-Book*, Elsevier Health Sciences.

TARASCO, M., CORDELIERES, F. P., CANCELA, M. L. & LAIZÉ, V. 2020. ZFBONE: An ImageJ toolset for semi-automatic analysis of zebrafish bone structures. *Bone,* 138**,** 115480.

TERA, T. D. M., NASCIMENTO, R. D., PRADO, R. F. D., SANTAMARIA, M. P. & JARDINI, M. A. N. 2014. Immunolocalization of markers for bone formation during guided bone regeneration in osteopenic rats. Journal of Applied Oral Science, 22, 541-553.

VALVERDE, P., ZHANG, J., FIX, A., ZHU, J., MA, W., TU, Q. & CHEN, J. 2008. Overexpression of bone sialoprotein leads to an uncoupling of bone formation and bone resorption in mice. Journal of bone and mineral research, 23, 1775-1788.

VINCENT, K. & DURRANT, M. C. 2013. A structural and functional model for human bone sialoprotein. *Journal of Molecular Graphics and Modelling,* 39**,** 108-117.

WANG, X.-M., QIU, Z.-Y. & CUI, H. 2019. Mineralized Collagen Bone Graft Substitutes, Woodhead Publishing.

WATSON, E. C. & ADAMS, R. H. 2018. Biology of bone: the vasculature of the skeletal system. Cold Spring Harbor perspectives in medicine, 8, a031559.

YANG, W., YAO, C., CUI, Z., LUO, D., LEE, I.-S., YAO, J., CHEN, C. & KONG, X. 2016. Poly (acrylic acid)-regulated synthesis of rod-like calcium carbonate nanoparticles for inducing the osteogenic differentiation of MC3T3-E1 cells. International Journal of Molecular Sciences, 17, 639.

YANG, X., LI, Y., LIU, X., HE, W., HUANG, Q. & FENG, Q. 2020. Nanoparticles and their effects on differentiation of mesenchymal stem cells. Biomaterials Translational, 1, 58.

YASAR, F., APAYDıN, B. & YıLMAZ, H.-H. 2012. The effects of image compression on quantitative measurements of digital panoramic radiographs. *Medicina oral, patologia oral y cirugia bucal,* 17**,** e1074.

ZHAO, X., NG, S., HENG, B. C., GUO, J., MA, L., TAN, T. T. Y., NG, K. W. & LOO, S. C. J. 2013. Cytotoxicity of hydroxyapatite nanoparticles is shape and cell dependent. Archives of toxicology, 87, 1037-1052.